THE JOURNAL OF PHYSICAL CHEMISTRY C

Article

pubs.acs.org/JPCC

Mechanically Induced Light Emission and Infrared-Laser-Induced Upconversion in the Er-Doped CaZnOS Multifunctional Piezoelectric Semiconductor for Optical Pressure and Temperature Sensing

Hanlu Zhang,[†,‡,§] Dengfeng Peng,[‡,§] Wei Wang,[‡] Lin Dong,[*,†,‡] and Caofeng Pan[*,‡]

[†]School of Materials Science & Engineering, Zhengzhou University, Zhengzhou 450001, P.R. China

[‡]Beijing Institute of Nanoenergy and Nanosystems, Chinese Academy of Sciences, Beijing 100083, P.R. China

Supporting Information

ABSTRACT: In this study, we report an Er-doped quaternary piezoelectric semiconductor CaZnOS:Er^{3+} which shows both mechanoluminescence and upconversion luminescence properties. Under mechanical stimulation, green light emission can be observed by the naked eye from a flexible film fabricated by encapsulating CaZnOS:Er^{3+} particles between two polyethylene glycol terephthalate substrates. The integral emission intensity is proportional to applied pressure, making CaZnOS:Er^{3+} suitable for dynamic pressure sensing applications. Moreover, the doped sample also shows bright visible emission with near-infrared (980 nm) excitation. The fluorescence intensity ratio between two upconversion emission bands corresponding to $^2H_{11/2}$, $^4S_{3/2} \rightarrow {}^4I_{15/2}$ transitions of Er^{3+} is sensitive to the variation of temperature. As a multifunctional optical material, CaZnOS:Er^{3+} could be used to not only visualize two-dimensional pressure distribution, through mechanically induced emission, but also sense temperature via the upconversion (UC) luminescence. This work provides a novel kind of multifunctional luminescent material for the development of integrated and coupling devices.

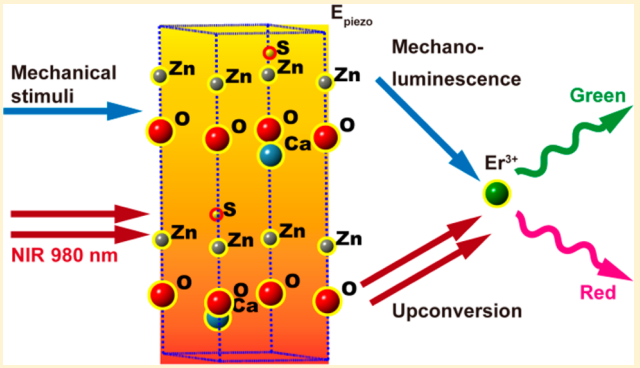

INTRODUCTION

Functional materials capable of sensing pressure and temperature based on optical methods may find their great applications in future intelligent sensors, human−machine interfaces, and robotics, which are hence not only exciting scientific topics but also technologically compelling.[1−7] Recently, intelligent materials with mechanically induced light emission properties, or so-called mechanoluminescence (ML), have been intensively investigated due to their uniquely inherent ability of emitting visible light under mechanical stimuli and their promising applications for optical force/pressure detection.[7−14] Meanwhile, upconversion (UC) luminescent materials that convert long-wavelength radiations into shorter wavelength emissions are vigorously studied for optical-based temperature sensing and other scientific objectives.[15−25] A material that exhibits both ML and UC properties might find interesting applications in visualizing pressure and temperature distribution, which is meaningful for developing highly integrated sensing systems.

Piezoelectric semiconductors (e.g., ZnO, GaN, CdS, and ZnS) have rich multifunctional physics, and their optical, electrical, and mechanical characteristics are capable of integration and coupling to originate new interesting effects, such as peizotronics and piezo-phototronics. The devices based on these effects have resulted in their widespread applications in photonics, electronics, sensors, and energy harvest.[26−34] The quaternary piezoelectric semiconductor CaZnOS first reported in 2003 is considered to be a good host material for luminescent centers due to its chemical and thermal stability, wide band gap, and high piezoelectricity which is pivotal for piezoelectric-induced ML emissions.[35−40] On the other hand, the Er^{3+} ion is one of the most studied rare earth luminescence centers with UC ability.[41,42] Temperature sensing based on the fluorescence intensity ratio (FIR) between $^2H_{11/2}$ and $^4S_{3/2} \rightarrow {}^4I_{15/2}$ transitions of Er^{3+} has been demonstrated with the advantages in noncontact measurements and the immunity to electromagnetic interferences.[43,44] In the present work, for the first time, we simultaneously realize ML and UC multifunctional properties in Er-doped piezoelectric semiconducting material CaZnOS and demonstrate its potential applications in pressure and temperature sensing.

EXPERIMENTAL SECTION

Preparation of CaZnOS:Er^{3+}. The CaZnOS:Er^{3+} particles were prepared via a solid-state reaction at high temperature. Appropriate ratios of raw materials including $CaCO_3$ (99.99%

Received: October 21, 2015
Revised: November 21, 2015

ACS Publications © XXXX American Chemical Society

DOI: 10.1021/acs.jpcc.5b10302
J. Phys. Chem. C XXXX, XXX, XXX−XXX

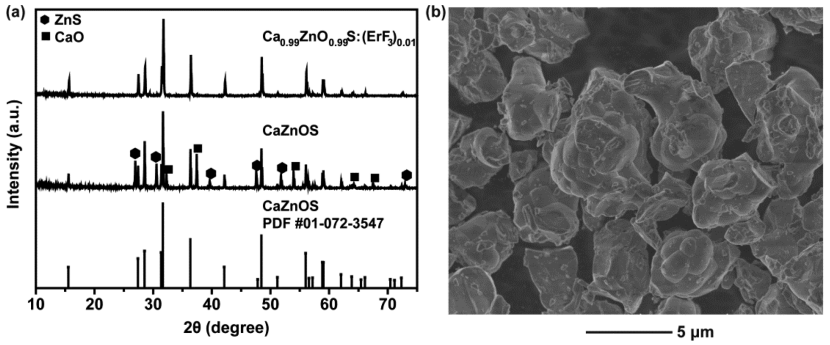

Figure 1. (a) XRD patterns of prepared $Ca_{0.99}ZnO_{0.99}S:(ErF_3)_{0.01}$ and CaZnOS samples together with the standard XRD pattern of CaZnOS. (b) An FESEM image of the $Ca_{0.99}ZnO_{0.99}S:(ErF_3)_{0.01}$ sample.

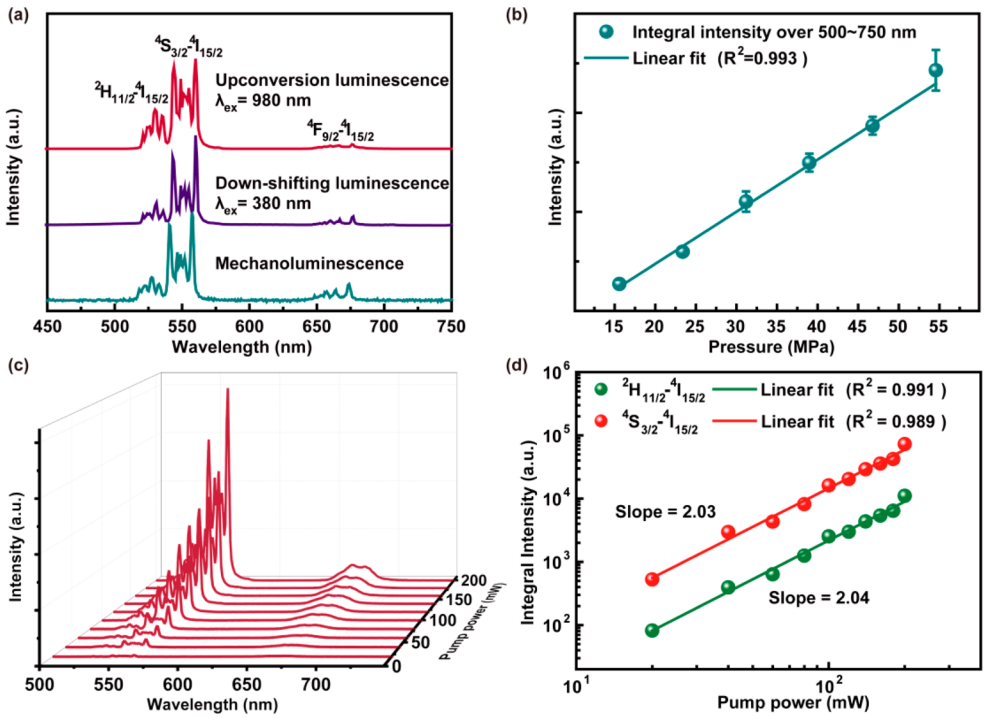

Figure 2. (a) Upconversion, down-shifting, and mechanoluminescence spectra of CaZnOS:Er^{3+}. (b) The linear correlation between the integral ML intensity and load pressure. (c) The UC emission spectra under the excitation of the 980 nm laser with different pump power. (d) UC emission intensity of the two green emission bands versus the pump power, indicating the two photons involved in the UC process.

in purity, Sinopharm Chemical Reagent Co.), ZnS (99.99% in purity, Aladdin), and ErF_3 (chemically synthetic) powders were thoroughly mixed by wet grinding (typically 1 mol % ErF_3 and 99 mol % $CaCO_3$ with respect to ZnS), employing ethanol as the dispersion medium. Then the dried powder mixture was loaded into a corundum crucible and sintered at 1000−1100 °C under an Ar atmosphere for 3 h. The sintered product was cooled to room temperature in the furnace and ground again into powders for subsequent characterizations and use. The nondoped CaZnOS particles were prepared likewise except for that no ErF_3 was added in raw materials.

Materials Characterizations. The crystal structure of prepared particles was examined by X-ray diffraction (XRD) using an X-ray diffractometer (PANalytical X'Pert^3 Powder) with the Cu Kα radiation. The morphology was characterized through a field emission scanning electron microscope (FESEM; Hitachi SU8020). The elementary composition was investigated by energy-dispersive X-ray spectroscopy (EDS, EDAX TEAM EDS). Down-shifting and UC spectra at room temperature were recorded by a fluorescence spectrometer (FLS980, Edinburgh Instruments) excited with a Xe lamp and 980 nm laser, respectively. The temperature-dependent and pump power-dependent UC spectra were collected by another fluorescence spectrometer (Hitachi F-7000) with additional temperature control unit.

Device Fabrication and ML Measurement. To evaluate the ML feature of CaZnOS:Er^{3+}, a homogeneous layer of obtained particles (0.3−0.5 g, dispersed in ethanol or in poly(methyl methacrylate):anisole solution for homogeneous deposition) was heat-sealed between two flexible and transparent 5 cm × 5 cm squared polyethylene glycol terephthalate (PET) thin films (each with thickness of ∼15 μm and covered by thermoplastics in one side). The ML emission of this composite film was detected by an in-house assembled ML measurement apparatus, in which a whole-steel stylus fixed on a linear motor (Linmot E1100) was used to apply periodically sliding force on the film that was supported by an acrylic sheet. The value of applied force could be tuned through three-

DOI: 10.1021/acs.jpcc.5b10302
J. Phys. Chem. C XXXX, XXX, XXX−XXX

Scheme 1. Luminescence Mechanisms of the ① UC, ② DS, and ③ ML Processes

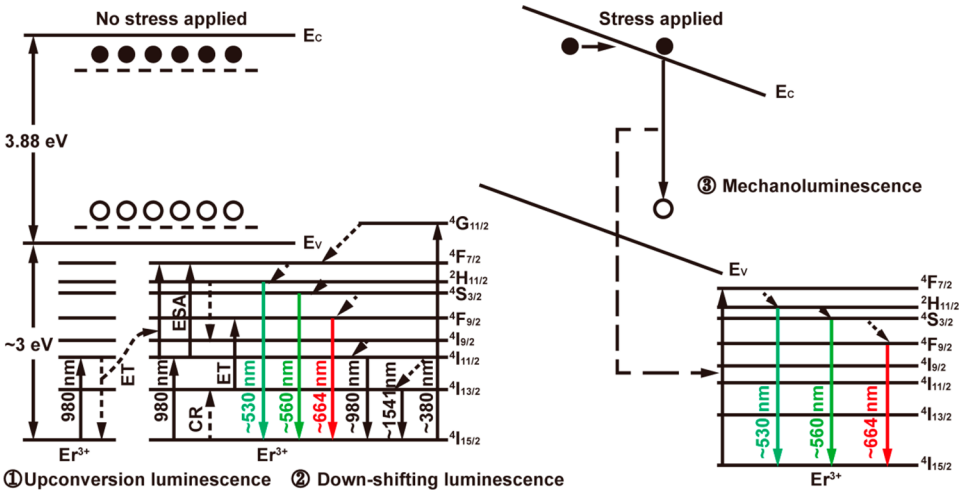

dimensional mechanical stages and be monitored by a force sensor (ATI Nano17), and a fiber optic spectrometer (Ocean Optics QE65pro) was employed to record the ML emission spectra. The pressure distribution image was captured by long-exposure photography or by accumulating frames in mechanoluminescence videos.

RESULTS AND DISCUSSION

Crystal Structure and Morphology. Figure 1a shows X-ray diffraction (XRD) patterns of prepared $Ca_{0.99}ZnO_{0.99}S:(ErF_3)_{0.01}$ particles together with the nondoped CaZnOS sample and the standard Powder Diffraction File card of CaZnOS (PDF #01-072-3547) for comparison.

Both samples were sintered at 1050 °C for 3 h. Some obvious peaks from unreacted ZnS and CaO are found appearing in the nondoped sample, which is consistent with the previous report,[45] while these impurities are largely suppressed and dispelled when ErF_3 is introduced. The XRD results reveal that the doping of ErF_3 may promote the formation of the CaZnOS phase at 1050 °C. Besides, the comparison among XRD patterns of samples sintered at different temperatures reveals that 1050 °C is proper for reaction: for the sample prepared at 1000 °C, the reaction is not complete; while for the sample prepared at 1100 °C, an additional CaS phase appears (Figure S1 in Supporting Information), which is also consistent with the previous report.[46] The FESEM image given in Figure 1b shows the size of the obtained particles was about 2−4 μm. EDS data confirm that the sample contains Ca, Zn, O, S, and Er elements (Figure S2 in Supporting Information), and the C peak may be described to the conductive carbon paste utilized to immobilize the sample.

Spectroscopic Studies. Prepared CaZnOS:Er^{3+} simultaneously possesses down-shifting (DS), UC, and ML luminescence properties. Figure 2a gives the comparison of the three kinds of luminescence spectra from $Ca_{0.99}ZnO_{0.99}S:(ErF_3)_{0.01}$, with the UC spectrum collected under the 980 nm laser excitation, DS spectrum collected under the 380 nm wavelength excitation, and ML spectrum collected under the load force of 15 N. The main emission bands and peaks are basically consistent in these three spectra, indicating that all three types of emission processes originated from the same activators of Er^{3+} ions. In the spectra, two main green emission bands located at 515−535 nm and 535−565 nm can be assigned to $^2H_{11/2}$, $^4S_{3/2} \rightarrow {}^4I_{15/2}$ transitions, and a weak red emission band located at 649−679 nm assigned to $^4F_{9/2} \rightarrow {}^4I_{15/2}$ of the Er^{3+} ion.[47] Stark splitting results in the generation of multiple peaks in each emission band.[48] In the ML spectrum, the relative intensity of the red emission with respect to the two green emissions seems to be higher than that in the DS and UC photoluminescence spectra, which may be attributed to the different wavelength responses between the different spectrometers we used for ML, DS, and UC measurements (specific instrument types are seen in the Experimental Section). The relationship between the ML intensity and the value of load pressure was investigated by applying different forces onto the composite film containing CaZnOS:Er^{3+} particles and collecting corresponding ML signals. The wavelength interval was set to 500−750 nm which covered the full emissive wavelength. Figure 2b shows a linear increase in the integral emission intensity over the wavelength interval with the increase of the applied force/pressure, which is consistent with the established theory,[49] indicating that this material is applicable in force/pressure sensing. Three typical ML spectra of the sample under different applied force are given as Figure S3 in the Supporting Information for intuitional comparison.

The excitation-intensity-dependent UC emission of the sample was further investigated upon the pumping power. In UC processes, the output emission intensity is proportional to the nth power of the excitation intensity, where n is the number of incident photons required to produce an UC photon.[41] Under the excitation of an invisible 980 nm laser, the emission intensity increases monotonously with the pumping power from 20 to 200 mW (Figure 2c). For the two main green Er^{3+} emission bands ($^2H_{11/2} \rightarrow {}^4I_{15/2}$, $^4S_{3/2} \rightarrow {}^4I_{15/2}$), the value of n is 2.03 and 2.04, respectively, according to the linear fitting result in the double logarithmic plots of the emission intensity versus the pump power (Figure 2d), indicating that two incident photons are involved in these two UC processes.[17] This result would help us to understand the underlying luminescence mechanism as discussed below (Scheme 1).

Luminescence Mechanisms. Possible mechanisms for the three luminous processes are illustrated in Scheme 1. For the UC process, an Er^{3+} ion at the ground state $^4I_{15/2}$ absorbs an incident 980 nm photon and is excited to the $^4I_{11/2}$ level; sequentially it is further excited to populate the $^4F_{7/2}$ level through excited state absorption (ESA) or energy transfer (ET)

DOI: 10.1021/acs.jpcc.5b10302
J. Phys. Chem. C XXXX, XXX, XXX−XXX

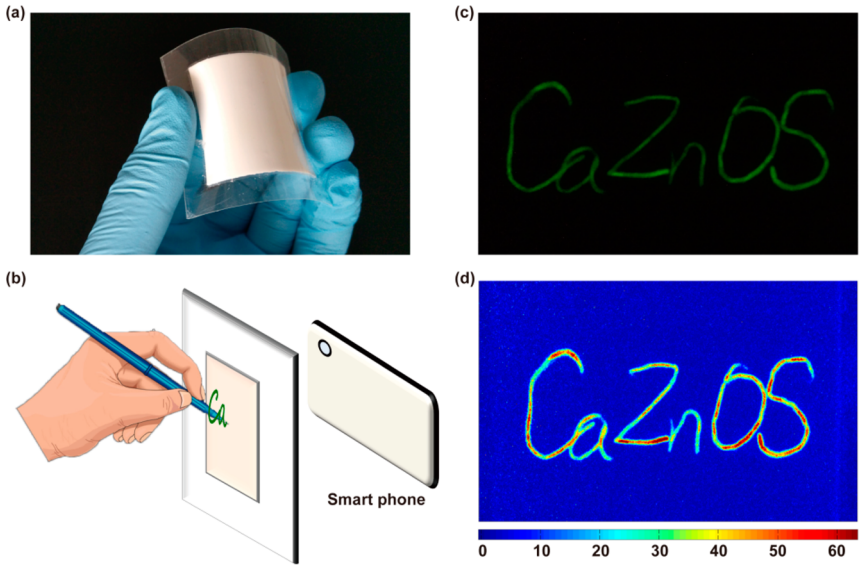

Figure 3. (a) Photograph of the fabricated flexible thin-film device containing a layer of CaZnOS:Er^{3+} particles. (b) The schematic illustration of the handwritten trajectory recording process. (c) Visualized handwritten trajectory through the long-exposure photography captured ML image (exposure time: 5 s). (d) Relative pressure distribution evaluated from the gray scale value mapping of the ML image.

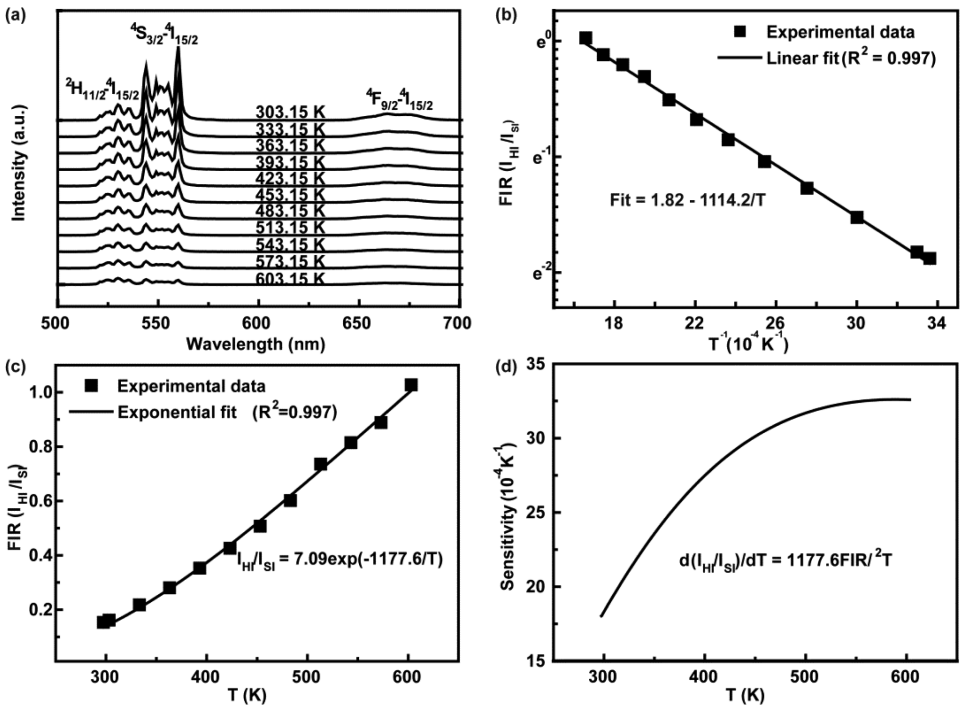

Figure 4. Temperature sensing based on the UC luminescence. (a) UC emission spectra at different temperatures. (b) The fluorescence intensity ratio (FIR) between the emissions from $^2H_{11/2} \rightarrow {}^4I_{15/2}$ and $^4S_{3/2} \rightarrow {}^4I_{15/2}$ as a function of reciprocal absolute temperature. (c) FIR versus the absolute temperature, showing an exponential characteristic. (d) The sensitivity of temperature sensing as a function of the temperature.

with the absorption of another 980 nm photon.[50] The nonradiative relaxation of Er^{3+} ions from $^4F_{7/2}$ populates the $^2H_{11/2}$ and $^4S_{3/2}$ levels, and the radiative decays of $^2H_{11/2}$ and $^4S_{3/2} \rightarrow {}^4I_{15/2}$ result in intense emissions at two green wavelength ranges. For the down-shifting process, Er^{3+} ions at the ground state of $^4I_{15/2}$ can be excited to the $^4G_{11/2}$ level by absorbing incident 380 nm photons, and consequently a series of nonradiative relaxations and radiative decays give rise to the emission of visible green light; moreover, invisible near-infrared ray (NIR) emissions peaking at 980 nm ($^4I_{11/2} \rightarrow {}^4I_{15/2}$) and 1541 nm ($^4I_{13/2} \rightarrow {}^4I_{15/2}$) were also detected in the DS process (Figure S4 in the Supporting Information). The NIR emission is in the range of the commonly used telecommunication window,[51] showing the potential applicability of CaZnOS:Er^{3+} in optical communications.

For the ML process, a possible mechanism is elucidated by the piezo-photonic effect.[37,40,49,52,53] As the host material CaZnOS is a highly piezoelectric wide band gap semiconductor (d_{33} = 38 pm V^{-1}, E_g = 3.88 eV),[36,48] inner crystal piezo potential will tilt the conduction and valence bands of CaZnOS when stress is applied to the CaZnOS:Er^{3+}. Consequently, the

DOI: 10.1021/acs.jpcc.5b10302
J. Phys. Chem. C XXXX, XXX, XXX−XXX

trapped electrons in the upper electron defect state of CaZnOS become much easier to be detrapped and released into the conduction band. Then a nonradioactive recombination occurs between detrapped electrons and holes by transferring energy to Er^{3+} ions at the ground state of $^4I_{15/2}$ to populate the $^4F_{7/2}$ level. The nonradiative relaxation of Er^{3+} ions from the excited $^4F_{7/2}$ level to lower levels and the following radiative decays to the ground state give rise to the visible light emissions.

Pressure Mapping. A thin-film device that contains a homogeneous layer of CaZnOS:Er^{3+} particles is fabricated for pressure sensing and visualization via the ML. As presented in Figure 3a, the composite film is flexible that can be bended to a large angle, and the particle layer is fixed and sealed in the sandwich-like structured middle layer, forming a robust device for further measurements.

The pressure distribution visualization ability of this thin-film device was demonstrated by a handwritten trajectory recording process as illustrated in Figure 3b. A commercial smart phone with the long-exposure photography function, which can record the motion trail of a single-point illuminant in the dark by prolonging photography exposure time, was used to capture the ML emission when a string of letters "CaZnOS" was written on the thin-film device attached on an acrylic sheet. The handwritten trajectory was visualized through the recorded long-exposure ML image from CaZnOS:Er^{3+} particles under the pressure of the ball-point pen with a ball of 0.7 mm in diameter and is shown in Figure 3c. It should be noted that the pressure-induced luminescence from one touch spot will fade away in a very short time (<15 ms), and to get such a trajectory image, the exposure time of the camera on the smart phone needs to be set long enough (5 s) to collect all the emitted light from each spot during the whole signature process. According to the previous discussion on the linear relationship between the ML intensity and localized applied pressure, the spatial distribution of the writing force/pressure can be derived from the ML intensity, which is relatively evaluated through the gray-scale value map of the visualized handwritten trajectory image as shown in Figure 3d. Via such an optical method, pressure distribution can be conveniently visualized and recorded without any specialized or sophisticated equipment, which is meaningful for developing smart human−machine interfaces.

Temperature Sensing. The multifunctional CaZnOS:Er^{3+} can not only visualize pressure distribution via its ML property but also implement temperature sensing via its UC luminous process. Figure 4a shows the UC emission spectra for $Ca_{0.99}ZnO_{0.99}S:(ErF_3)_{0.01}$ at the temperature range of 303.15−603.15 K under 980 nm excitation with the pumping power of 0.2 W. With the increase of temperature, the positions of the two green UC emission bands ($^2H_{11/2}$, $^4S_{3/2} \rightarrow {}^4I_{15/2}$) have no change; however, the fluorescence intensity ratio (FIR) of these two bands varies which is normally caused by the enhancements of nonradiative relaxation, endowing the sample with the ability of temperature sensing. The dependence of this FIR on the temperature can be theoretically inferred. First, since the energy gap between the $^2H_{11/2}$ and $^4S_{3/2}$ is small (about 700−800 cm^{-1}), the relative population of the two levels quickly gets a thermal equilibrium and follows a Boltzmann distribution at a certain temperature.[54] Second, the intensity of fluorescence is proportional to the population of the corresponding energy level. Therefore, the FIR of the two green UC emissions from $^2H_{11/2}$ and $^4S_{3/2}$ can be given as follows[17,54,55]

$$\mathrm{FIR}\left(\frac{I_{HI}}{I_{SI}}\right) = \frac{N(^2H_{11/2})}{N(^2S_{3/2})} = \frac{g_H\sigma_H\omega_H}{g_S\sigma_S\omega_S}\exp\left(\frac{-\Delta E}{k_BT}\right) = C\exp\left(\frac{-\Delta E}{k_BT}\right) \quad (1)$$

where I_{HI} and I_{SI} are the integral intensities of the $^2H_{11/2} \rightarrow {}^4I_{15/2}$ (520−539 nm) and $^4S_{3/2} \rightarrow {}^4I_{15/2}$ (539−570 nm), respectively. N, g, σ, and ω are the number of Er^{3+} ions, the degeneracy, the emission cross-section, and the angular frequency of fluorescence transitions from $^2H_{11/2}$, $^4S_{3/2}$ levels to the $^4I_{15/2}$ level, respectively. ΔE is the energy gap between $^2H_{11/2}$ and $^4S_{3/2}$ levels, k_B the Boltzmann constant, and T the absolute temperature, and the constant C represents the value of $g_H\sigma_H\omega_H/g_S\sigma_S\omega_S$. The subscripts of H, S, and I stand for the levels of $^2H_{11/2}$, $^4S_{3/2}$, and $^4I_{15/2}$ respectively.

Equation 1 can be rewritten as[56]

$$\ln(\mathrm{FIR}) = \ln(C) - \frac{A}{T} \quad (2)$$

where A represents the value of $\Delta E/k_B$. Figure 4b shows a plot of the logarithms of the FIR as a function of the reciprocal absolute temperature. The linear fit result gives a slope ($-A$) of about −1114.2, from which the energy gap ΔE can be estimated. Figure 4c plots the FIR corresponding to the temperature range of 303.15−603.15 K. The experimental data are exponential fitted to eq 1 with a well-matched result. The value of the coefficient C is 7.09 according to the fitting curve, and the value of A found by the exponential fit is −1177.6 which is close to the linear fit result in Figure 4b.

For the practical application of the temperature sensing ability, the temperature sensitivity S is an important reference value, which is defined as the variation of FIR with respect to temperature. According to eq 1, S can be deduced as[55]

$$S = \frac{d\mathrm{FIR}}{dT} = \mathrm{FIR}\frac{\Delta E}{k_BT^2} \quad (3)$$

Figure 4d plots the resultant curve of S value obtained from the derivation of the fitting curve of FIR in Figure 4c. In the detection range of 303.15−603.15 K, the value of S monotonously increases with temperature and reaches the maximum value of about 0.0033 K^{-1} at the temperature of 603.15 K. The monotonous zone and the maximum value of the sensitivity are comparable to those of other reports, given that no sensitizer is adopted in our sample.[17]

CONCLUSIONS

In summary, we originally demonstrate the multifunctionality of CaZnOS:Er^{3+} with ML, UC, and DS luminescent property for pressure and temperature sensing via an all-optical method. The integral ML intensity of CaZnOS:Er^{3+} is linearly related to applied force/pressure, hence the pressure distribution is visualized through the superposed ML intensity mapping acquired via long-exposure photography. Moreover, the fluorescence intensity ratio (FIR) of $^2H_{11/2}$ and $^4S_{3/2} \rightarrow {}^4I_{15/2}$ of Er^{3+} in the UC process is utilized to probe the temperature in the range of 303.15−603.15 K with a maximum sensitivity of 0.0033 K^{-1}. This work may find broad applications for future generations of intelligent sensors, electronic skins, autonomous robotics, and human−machine interfaces based on optical signals.

DOI: 10.1021/acs.jpcc.5b10302
J. Phys. Chem. C XXXX, XXX, XXX−XXX

■ ASSOCIATED CONTENT

Supporting Information

The Supporting Information is available free of charge on the ACS Publications website at DOI: 10.1021/acs.jpcc.5b10302.

XRD patterns of $Ca_{0.99}ZnO_{0.99}S:(ErF_3)_{0.01}$ particles prepared at different temperatures; EDS data of the sample; three typical ML spectra collected under different forces; the full down-shifting emission spectra of the sample including NIR range; the photograph of the UC luminescence from the fabricated thin-film device (Figure S5), and a final superposed image that presents the trajectory of handwriting (PDF)

A frame-accumulated video presents the ML process for pressure sensing (AVI)

■ AUTHOR INFORMATION

Corresponding Authors

*E-mail: ldong@zzu.edu.cn.

*E-mail: cfpan@binn.cas.cn. Tel.: +86-10-82854771.

Author Contributions

§These authors contributed equally to this work.

Notes

The authors declare no competing financial interest.

■ ACKNOWLEDGMENTS

The authors are thankful for the support from the "thousands talents" program for pioneer researcher and his innovation team, China; President Funding of the Chinese Academy of Sciences, National Natural Science Foundation of China (No. 51272238, 21321062, 51432005, and 61405040), the Innovation Talent Project of Henan Province (No. 13HASTIT020), Talent Project of Zhengzhou University (ZDGD13001), and Surface Engineering Key Lab of LIPCA. We thank Prof. Xusheng Wang and Dr. Jun Li at Tongji University for their generous assistance in spectroscopic measurements.

■ REFERENCES

(1) Chortos, A.; Bao, Z. N. Skin-Inspired Electronic Devices. *Mater. Today* **2014**, *17*, 321−331.

(2) Levi, A.; Piovanelli, M.; Furlan, S.; Mazzolai, B.; Beccai, L. Soft, Transparent, Electronic Skin for Distributed and Multiple Pressure Sensing. *Sensors* **2013**, *13*, 6578−6604.

(3) Tokarev, I.; Motornov, M.; Minko, S. Molecular-Engineered Stimuli-Responsive Thin Polymer Film: A Platform for the Development of Integrated Multifunctional Intelligent Materials. *J. Mater. Chem.* **2009**, *19*, 6932−6948.

(4) Pan, C. F.; Dong, L.; Zhu, G.; Niu, S. M.; Yu, R. M.; Yang, Q.; Liu, Y.; Wang, Z. L. High-Resolution Electroluminescent Imaging of Pressure Distribution Using a Piezoelectric Nanowire LED Array. *Nat. Photonics* **2013**, *7*, 752−758.

(5) Bao, R. R.; Wang, C. F.; Dong, L.; Yu, R. M.; Zhao, K.; Wang, Z. L.; Pan, C. F. Flexible and Controllable Piezo-Phototronic Pressure Mapping Sensor Matrix by ZnO NW/p-Polymer LED Array. *Adv. Funct. Mater.* **2015**, *25*, 2884−2891.

(6) Wang, X. D.; Dong, L.; Zhang, H. L.; Yu, R. M.; Pan, C. F.; Wang, Z. L. Recent Progress in Electronic Skin. *Adv. Sci.* **2015**, DOI: 10.1002/advs.201500169.

(7) Chandra, B. P.; Chandra, V. K.; Mahobia, S. K.; Jha, P.; Tiwari, R.; Haldar, B. Real-time Mechanoluminescence Sensing of the Amplitude and Duration of Impact Stress. *Sens. Actuators, A* **2012**, *173*, 9−16.

(8) Jha, P.; Chandra, B. P. Survey of the Literature on Mechanoluminescence from 1605 to 2013. *Luminescence* **2014**, *29*, 977−993.

(9) Xu, C. N.; Watanabe, T.; Akiyama, M.; Zheng, X. G. Artificial Skin to Sense Mechanical Stress by Visible Light Emission. *Appl. Phys. Lett.* **1999**, *74*, 1236−1238.

(10) Jeong, S. M.; Song, S.; Lee, S.-K.; Ha, N. Y. Color Manipulation of Mechanoluminescence from Stress-Activated Composite Films. *Adv. Mater.* **2013**, *25*, 6194−6200.

(11) Peng, D. F.; Chen, B.; Wang, F. Recent Advances in Doped Mechanoluminescent Phosphors. *ChemPlusChem* **2015**, *80*, 1209−1215.

(12) Liu, Y.; Xu, C. N. Influence of Calcining Temperature on Photoluminescence and Triboluminescence of Europium-Doped Strontium Aluminate Particles Prepared by Sol-gel Process. *J. Phys. Chem. B* **2003**, *107*, 3991−3995.

(13) Chandra, V. K.; Chandra, B. P. Suitable Materials for Elastico Mechanoluminescence-Based Stress Sensors. *Opt. Mater.* **2011**, *34*, 194−200.

(14) Olawale, D. O.; Dickens, T.; Sullivan, W. G.; Okoli, O. I.; Sobanjo, J. O.; Wang, B. Progress in Triboluminescence-Based Smart Optical Sensor System. *J. Lumin.* **2011**, *131*, 1407−1418.

(15) Song, E.-H.; Ding, S.; Wu, M.; Ye, S.; Xiao, F.; Dong, G.-P.; Zhang, Q.-Y. Temperature-Tunable Upconversion Luminescence of Perovskite Nanocrystals $KZnF_3:Yb^{3+},Mn^{2+}$. *J. Mater. Chem. C* **2013**, *1*, 4209−4215.

(16) Zheng, K. Z.; Liu, Z. Y.; Lv, C. J.; Qin, W. P. Temperature Sensor Based on the UV Upconversion Luminescence of Gd^{3+} in Yb^{3+}-Tm^{3+}-Gd^{3+} Codoped $NaLuF_4$ Microcrystals. *J. Mater. Chem. C* **2013**, *1*, 5502−5507.

(17) Dong, B.; Cao, B. S.; He, Y. Y.; Liu, Z.; Li, Z. P.; Feng, Z. Q. Temperature Sensing and In Vivo Imaging by Molybdenum Sensitized Visible Upconversion Luminescence of Rare-Earth Oxides. *Adv. Mater.* **2012**, *24*, 1987−1993.

(18) Zhou, J.; Liu, Q.; Feng, W.; Sun, Y.; Li, F. Y. Upconversion Luminescent Materials: Advances and Applications. *Chem. Rev.* **2015**, *115*, 395−465.

(19) Wang, F.; Liu, X. G. Recent Advances in the Chemistry of Lanthanide-Doped Upconversion Nanocrystals. *Chem. Soc. Rev.* **2009**, *38*, 976−989.

(20) Chen, B.; Qiao, X. S.; Peng, D. F.; Fan, X. P. Enhanced Luminescence of $NaY_{0.6-x}Ce_{0.1}Gd_{0.3}Eu_xF_4$ Nanorods by Energy Transfers between Ce^{3+}, Gd^{3+}, and Eu^{3+}. *J. Phys. Chem. C* **2014**, *118*, 30197−30201.

(21) Li, D. D.; Shao, Q. Y.; Dong, Y.; Jiang, J. Q. Anomalous Temperature-Dependent Upconversion Luminescence of Small-Sized $NaYF_4:Yb^{3+}$, Er^{3+} Nanoparticles. *J. Phys. Chem. C* **2014**, *118*, 22807−22813.

(22) Mahalingam, V.; Mangiarini, F.; Vetrone, F.; Venkatramu, V.; Bettinelli, M.; Speghini, A.; Capobianco, J. A. Bright White Upconversion Emission from $Tm^{3+}/Yb^{3+}/Er^{3+}$-Doped $Lu_3Ga_5O_{12}$ Nanocrystals. *J. Phys. Chem. C* **2008**, *112*, 17745−17749.

(23) Wang, B.; Sun, B.; Wang, X. M.; Ye, C. Q.; Ding, P.; Liang, Z. Q.; Chen, Z. G.; Tao, X. T.; Wu, L. Z. Efficient Triplet Sensitizers of Palladium(II) Tetraphenylporphyrins for Upconversion-Powered Photoelectrochemistry. *J. Phys. Chem. C* **2014**, *118*, 1417−1425.

(24) Lissau, J. S.; Gardner, J. M.; Morandeira, A. Photon Upconversion on Dye-Sensitized Nanostructured ZrO_2 Films. *J. Phys. Chem. C* **2011**, *115*, 23226−23232.

(25) Liu, T.; Bai, X.; Miao, C.; Dai, Q. L.; Xu, W.; Yu, Y. H.; Chen, Q. D.; Song, H. W. Yb_2O_3/Au Upconversion Nanocomposites with Broad-Band Excitation for Solar Cells. *J. Phys. Chem. C* **2014**, *118*, 3258−3265.

(26) Wang, X. D.; Zhou, J.; Song, J. H.; Liu, J.; Xu, N. S.; Wang, Z. L. Piezoelectric Field Effect Transistor and Nanoforce Sensor Based on a Single ZnO Nanowire. *Nano Lett.* **2006**, *6*, 2768−2772.

(27) Wang, Z. L.; Song, J. H. Piezoelectric Nanogenerators Based on Zinc Oxide Nanowire Arrays. *Science* **2006**, *312*, 242−246.

(28) Zhou, J.; Gu, Y. D.; Fei, P.; Mai, W. J.; Gao, Y. F.; Yang, R. S.; Bao, G.; Wang, Z. L. Flexible Piezotronic Strain Sensor. *Nano Lett.* **2008**, *8*, 3035−3040.

(29) Dong, L.; Niu, S. M.; Pan, C. F.; Yu, R. M.; Zhang, Y.; Wang, Z. L. Piezo-Phototronic Effect of CdSe Nanowires. *Adv. Mater.* **2012**, *24*, 5470−5475.
(30) Yu, R. M.; Dong, L.; Pan, C. F.; Niu, S. M.; Liu, H. F.; Liu, W.; Chua, S. J.; Chi, D. Z.; Wang, Z. L. Piezotronic Effect on the Transport Properties of GaN Nanobelts for Active Flexible Electronics. *Adv. Mater.* **2012**, *24*, 3532−3537.
(31) Wang, Z. L.; Zhu, G.; Yang, Y.; Wang, S. H.; Pan, C. F. Progress in Nanogenerators for Portable Electronics. *Mater. Today* **2012**, *15*, 532−543.
(32) Yang, Q.; Liu, Y.; Pan, C. F.; Chen, J.; Wen, X. N.; Wang, Z. L. Largely Enhanced Efficiency in ZnO Nanowire/p-Polymer Hybridized Inorganic/Organic Ultraviolet Light-Emitting Diode by Piezo-Phototronic Effect. *Nano Lett.* **2013**, *13*, 607−613.
(33) Wu, W. Z.; Wen, X. N.; Wang, Z. L. Taxel-Addressable Matrix of Vertical-Nanowire Piezotronic Transistors for Active and Adaptive Tactile Imaging. *Science* **2013**, *340*, 952−957.
(34) Wang, C. F.; Bao, R. R.; Zhao, K.; Zhang, T. P.; Dong, L.; Pan, C. F. Enhanced Emission Intensity of Vertical Aligned Flexible ZnO Nanowire/p-Polymer Hybridized LED Array by Piezo-Phototronic Effect. *Nano Energy* **2015**, *14*, 364−371.
(35) Petrova, S. A.; Mar'evich, V. P.; Zakharov, R. G.; Selivanov, E. N.; Chumarev, V. M.; Udoeva, L. Y. Crystal Structure of Zinc Calcium Oxysulfide. *Dokl. Chem.* **2003**, *393*, 255−258.
(36) Sambrook, T.; Smura, C. F.; Clarke, S. J.; Ok, K. M.; Halasyamani, P. S. Structure and Physical Properties of the Polar Oxysulfide CaZnOS. *Inorg. Chem.* **2007**, *46*, 2571−2574.
(37) Wang, Z. L. Towards Self-Powered Nanosystems: From Nanogenerators to Nanopiezotronics. *Adv. Funct. Mater.* **2008**, *18*, 3553−3567.
(38) Zhang, J.-C.; Xu, C. N.; Kamimura, S.; Terasawa, Y.; Yamada, H.; Wang, X. S. An Intense Elastico-Mechanoluminescence Material CaZnOS:Mn^{2+} for Sensing and Imaging Multiple Mechanical Sstresses. *Opt. Express* **2013**, *21*, 12976−12986.
(39) Tu, D.; Xu, C. N.; Fujio, Y. Intense Red Emitting Mechanoluminescence from CaZnOS:Mn,Li with c-Axis Preferred Orientation. *J. Adv. Dielectr.* **2014**, *04*, 1450017.
(40) Chandra, B. P.; Chandra, V. K.; Jha, P. Microscopic Theory of Elastico-Mechanoluminescent Smart Materials. *Appl. Phys. Lett.* **2014**, *104*, 031102.
(41) Peng, D. F.; Zou, H.; Xu, C. N.; Wang, X. S.; Yao, X.; Lin, J.; Sun, T. T. Upconversion Luminescence, Ferroelectrics and Piezoelectrics of Er Doped $SrBi_4Ti_4O_{15}$. *AIP Adv.* **2012**, *2*, 042187.
(42) Gong, S. Y.; Ren, Z. H.; Jiang, S.; Li, M.; Li, X.; Wei, X.; Xu, G.; Shen, G.; Han, G. R. Phase-Modified Up-Conversion Luminescence in Er-Doped Single-Crystal $PbTiO_3$ Nanofibers. *J. Phys. Chem. C* **2014**, *118*, 5486−5493.
(43) dos Santos, P. V.; de Araujo, M. T.; Gouveia-Neto, A. S.; Neto, J. A. M.; Sombra, A. S. B. Optical Temperature Sensing Using Upconversion Fluorescence Emission in Er^{3+}/Yb^{3+}-Codoped Chalcogenide Glass. *Appl. Phys. Lett.* **1998**, *73*, 578−580.
(44) Zou, H.; Li, J.; Wang, X. S.; Peng, D. F.; Li, Y. X.; Yao, X. Color-Tunable Upconversion Emission and Optical Temperature Sensing Behaviour in Er-Yb-Mo Codoped $Bi_7Ti_4NbO_{21}$ Multifunctional Ferroelectric Oxide. *Opt. Mater. Express* **2014**, *4*, 1545−1554.
(45) Duan, C. J.; Delsing, A. C. A.; Hintzen, H. T. Photoluminescence Properties of Novel Red-Emitting Mn^{2+}-Activated MZnOS (M = Ca, Ba) Phosphors. *Chem. Mater.* **2009**, *21*, 1010−1016.
(46) Qiu, Z. X.; Rong, C. Y.; Zhou, W. L.; Zhang, J. L.; Li, C. Z.; Yu, L. P.; Liu, S. B.; Lian, S. X. A Strategy for Synthesizing CaZnOS:Eu^{2+} Phosphor and Comparison of Optical Properties with CaS:Eu^{2+}. *J. Alloys Compd.* **2014**, *583*, 335−339.
(47) Wang, F.; Liu, X. G. Upconversion Multicolor Fine-Tuning: Visible to Near-Infrared Emission from Lanthanide-Doped $NaYF_4$ Nanoparticles. *J. Am. Chem. Soc.* **2008**, *130*, 5642−5643.
(48) Zhang, Z. J.; Feng, A.; Chen, X. Y.; Zhao, J. T. Photoluminescence Properties and Energy Levels of RE (RE = Pr, Sm, Er, Tm) in Layered-CaZnOS Oxysulfide. *J. Appl. Phys.* **2013**, *114*, 213518.
(49) Chandra, B. P.; Chandra, V. K.; Jha, P. Piezoelectrically-Induced Trap-Depth Reduction Model of Elastico-Mechanoluminescent Materials. *Phys. B* **2015**, *461*, 38−48.
(50) Zhang, Y.; Hao, J. H.; Mak, C. L.; Wei, X. H. Effects of Site Substitutions and Concentration on Upconversion Luminescence of Er^{3+}-Doped Perovskite Titanate. *Opt. Express* **2011**, *19*, 1824−1829.
(51) Stouwdam, J. W.; van Veggel, F. C. J. M. Near-Infrared Emission of Redispersible Er^{3+}, Nd^{3+}, and Ho^{3+} Doped LaF_3 Nanoparticles. *Nano Lett.* **2002**, *2*, 733−737.
(52) Wang, X. D.; Zhang, H. L.; Yu, R. M.; Dong, L.; Peng, D. F.; Zhang, A. H.; Zhang, Y.; Liu, H.; Pan, C. F.; Wang, Z. L. Dynamic Pressure Mapping of Personalized Handwriting by a Flexible Sensor Matrix Based on the Mechanoluminescence Process. *Adv. Mater.* **2015**, *27*, 2324−2331.
(53) Chandra, V. K.; Chandra, B. P.; Jha, P. Strong Luminescence Induced by Elastic Deformation of Piezoelectric Crystals. *Appl. Phys. Lett.* **2013**, *102*, 241105.
(54) Yang, X. X.; Fu, Z. L.; Yang, Y. M.; Zhang, C. P.; Wu, Z. J.; Sheng, T. Q. Optical Temperature Sensing Behavior of High-Efficiency Upconversion: Er^{3+}−Yb^{3+} Co-Doped $NaY(MoO_4)_2$ Phosphor. *J. Am. Ceram. Soc.* **2015**, *98*, 2595−2600.
(55) Zhou, S. S.; Deng, K. M.; Wei, X. T.; Jiang, G. C.; Duan, C. K.; Chen, Y. H.; Yin, M. Upconversion Luminescence of $NaYF_4$: Yb^{3+}, Er^{3+} for Temperature Sensing. *Opt. Commun.* **2013**, *291*, 138−142.
(56) Yang, Y. M.; Mi, C.; Jiao, F. Y.; Su, X. Y.; Li, X. D.; Liu, L. L.; Zhang, J.; Yu, F.; Liu, Y. Z.; Mai, Y. H. A Novel Multifunctional Upconversion Phosphor: Yb^{3+}/Er^{3+} Codoped La_2S_3. *J. Am. Ceram. Soc.* **2014**, *97*, 1769−1775.

DOI: 10.1021/acs.jpcc.5b10302
J. Phys. Chem. C XXXX, XXX, XXX−XXX